Ratchetaxis in Channels: Entry Point and Local Asymmetry Set Cell Directions in Confinement

Emilie Le Maout, Simon Lo Vecchio, Praveen Kumar Korla, Jim Jinn-Chyuan Sheu, Daniel Riveline

Ratchetaxis in channels: entry point and local asymmetry set cell directions in confinement.

Emilie Le Maout[1-5]*, Simon Lo Vecchio[1-5]*, Praveen Kumar Korla[7], Jim Jinn-Chyuan Sheu[7-9], Daniel Riveline[1-5†]

[1]Laboratory of Cell Physics ISIS/IGBMC, CNRS and University of Strasbourg, Strasbourg, France.
[2]Institut de Génétique et de Biologie Moléculaire et Cellulaire, Illkirch, France.
[3]Centre National de la Recherche Scientifique, UMR7104, Illkirch, France.
[4]Institut National de la Santé et de la Recherche Médicale, U964, Illkirch, France.
[5]Université de Strasbourg, Illkirch, France.
[6]Institute of Biomedical Sciences, National Sun Yatsen University, Kaohsiung 80242, Taiwan. [7]School of Chinese Medicine, China Medical University, Taichung 40402, Taiwan.
[8]Department of Health and Nutrition Biotechnology, Asia University, Taichung 41354, Taiwan. [9]Department of Biotechnology, Kaohsiung Medical University, Kaohsiung 80708, Taiwan.
[†]Corresponding author: riveline@unistra.fr
*Co-first authorship

ABSTRACT

Cell motility is essential in a variety of biological phenomena ranging from early development to organ homeostasis and diseases. This phenomenon has mainly been studied and characterized on flat surfaces in vitro, *whereas such conditions are rarely observed* in vivo. *Recently, cell motion in 3D microfabricated channels was reported to be possible, and it was shown that confined cells push on walls. However, rules setting cell directions in this context have not yet been characterized. Here, we show by using assays that* ratchetaxis *operates in 3D ratchets in fibroblasts and epithelial cancerous cells. Open ratchets rectify cell motion, whereas closed ratchets impose direct cell migration along channels set by the cell orientation at the channel entry point. We also show that nuclei are pressed in constriction zones through mechanisms involving dynamic asymmetries of focal contacts, stress fibers, and intermediate filaments. Interestingly, cells do not pass these constricting zones when they contain a defective keratin fusion protein implicated in squamous cancer. By combining* ratchetaxis *with chemical gradients, we finally report that cells are sensitive to local asymmetries in confinement and that topological and chemical cues may be encoded differently by cells. Overall, our ratchet channels could mimic small blood vessels where cells such as circulating tumor cells (CTCs) are confined: cells can probe local asymmetries that determine their entry into tissues and their subsequent direction. Our results shed light on invasion mechanisms in cancer.*

INTRODUCTION

Directed cell migration plays a key role in many physiological, pathological and developmental processes [1–4]. Its dynamics have been widely studied, mainly under conditions that are far from physiological conditions on 2D flat surfaces [5,6]. However, in tissues or capillaries, cells are often confined, and their cytoskeleton and organelles undergo deformation and reshaping to bypass obstacles and maintain motion. For example, circulating

tumor cells (CTCs) transported by blood flows *in vivo* can be trapped in small blood vessels in capillary networks. They can remain in the same place for some time, and this mechanical confinement can lead to their remodeling and entry into neighboring tissues through extravasation [7,8]. These situations can also be observed *in vivo* in small veins and venules where microscopic venous valves (MVVs) are present [9], introducing natural obstacles based on their dimensions. These physiological contexts call for new studies addressing motion in controlled geometries and environments.

To test cell motion in confined situations *in vitro,* cell migration has been studied in microfabricated structures. It has been shown that motility in microchannels with nonadhesive walls may be distinct from motion on a flat surface, as cells "push" against walls [10–12] and exhibit high persistence in straight channels [13,14]. More broadly, it has been reported that confinement, adhesion, and contractility contribute to determining the type of motion performed by a cell, which can shift from mesenchymal to ameboid types of motility. Depending on localization in the phase diagram, cells can undergo different types of migration involving distinct cellular structures, ranging from focal adhesion-based motility to retrograde flow-mediated motion, which are associated with changes in cell shape and cell speed [15]. A recent study also indicated that the migration of T cells was related to local asymmetries in confined channels. Close contact with a curved channel mediates actin flow-related shear stress, which promotes cell motion in both the presence and absence of adhesion [16]. Altogether, these findings indicate that different types of cell motion in confined situations can be governed by similar rules. The observation of the cellular structures related to such migration has enlarged the scope of the understanding of cell motility, placing symmetry and direction as central arguments.

Confinement can also impede the passage of cells. The principle of a bottleneck implies the issue of an obstacle along the way and poses the question of how it can be untrapped by cellular structures. It has been reported that the nucleus, as a large organelle, can undergo significant deformation with potential biological functions or effects such as rupture [17,18]. In addition, actin accumulation at bottlenecks has been reported and is hypothesized to mediate nuclear deformation [19]. Nevertheless, it is not clear how the cell cytoskeleton reorganizes to adapt to local asymmetries in channels or constricting zones. In addition, in some squamous cancers, cells are known to exhibit defective keratin, an intermediate filament that is essential to shape the scaffold surrounding the nucleus [20]. The defects in these structures and their implications for motility in confined spaces have not been reported. Nuclei could potentially be trapped in these situations, and the cytoskeleton may be defective in their release.

Direction and obstacles are therefore key aspects of cell motility. Recently, *ratchetaxis* was proposed as a generic term for directed cell motion with externally induced local asymmetries. The principle consists of breaking locally cell symmetry at the scale of a cell. Polarity is then acquired, and the memory of polarity has a given timescale. Various realizations of ratchetaxis were performed with adhesive patterns and topological small heights [21–27]. Polarity is imposed through the distribution of focal contacts and/or constraints on the nucleus. Cell motion has been shown to be rectified with controlled efficiency. To address the same questions in 3D situations, we decided to test motion within *confined* geometries in a configuration close to the physiological conditions reported above, which can lead to different rules for setting cell directions and passing obstacles. We designed a setup involving periodic ratchets in channels [28]. The applied constriction zones were smaller than the nuclear dimensions.

Here, we study rules that determine cell directions and nucleus release in constriction zones. In this work, we show that periodic asymmetries direct cell motion when cells are confined in open channels. When totally confined, the direction of migration is exclusively determined by the cell entry point in the channel: cells cannot repolarize, and their trajectories are not biased by the cues provided by geometry. To characterize the cellular mechanisms involved in this directed motion, we next studied the dynamics of actin, focal contacts, the nucleus and the keratin array surrounding the nucleus when cells pass through bottlenecks. We report anisotropies in the distribution of cytoskeletal proteins with actin bundles located at the bottom and the top of the cell, between which the nucleus can be deformed. Focal contacts are mainly located at the channel wall, specifically at the junctions between ratchet units. The keratin array also exhibits an asymmetric distribution where keratin accumulates at the posterior of the nucleus, potentially to facilitate deformation. Finally, we combined a chemical gradient with a channel experiment, and we found that cells were able to sustain their migration when the gradient was removed only when the direction of anisotropy was not an obstacle; otherwise, the cells stopped migrating. Altogether, our results describe the migration and deformation of cells through confined spaces, paving the way for future works exploring cell motility in small blood capillaries *in vivo*.

METHODS

Microfabrication

SU-8 molds were prepared using standard UV-photolithography, following methods similar to those detailed in our previous methods paper [28]. Polydimethylsiloxane (PDMS, 1:10 w/w cross-linker:pre-polymer) (Sylgard 184 kit, Dow Corning, cat. DC184-1.1) was then poured and cured at 65°C for at least 4 hours.

Next, PDMS chips and glass coverslips were treated with oxygen plasma and bound together in two different ways depending on the configuration to be tested (closed or open) [28]: the microchannel chip faced upward for open channels, while it faced downward for the closed configuration. The PDMS and glass coverslips were then incubated overnight at 65°C to ensure proper binding and prevent any detachment or leakage.

Cell culture and migration assays

NIH3T3 (ATCC) cells were cultured in high-glucose Dulbecco's modified Eagle's medium (DMEM) (Fisher Scientific, cat. 11574486) with 10% bovine calf serum (BCS) (Sigma, cat. 12133C) and 1% penicillin-streptomycin.
HL60 cells were grown in suspension in RPMI 1640 (Gibco, cat. 22409031) supplemented with 40 µg/mL gentamycin and 10% fetal bovine serum (FBS) (Pan Biotech, cat. P30-3302).

CAL-27 cells were cultured in low-glucose DMEM (Fisher Scientific, cat. 11966-025) supplemented with 10% FBS (HyClone, cat. SH30109.03) and 1% penicillin-streptomycin.

For experiments in channels, the cells were detached using Trypsin-0.25% EDTA (Fisher Scientific, cat 11570626), centrifuged and resuspended in L-15 (Leibovitz Medium, Fisher Scientific, cat. 11540556) at the desired concentrations: for the open-channel configuration, 100 µL of a solution of 100,000 cells/mL was deposited on the PDMS motifs; for the closed channel configuration, a solution of 30,000,000 cells/mL was prepared, and 20 µL was injected into the chip reservoir.

Gradient formation

A BCS gradient was produced with two 1 mL syringes prepared with L-15 0.1% BCS and 10% BCS with TRITC-dextran (20 kDa, Sigma, cat. 73766). The flow rate of the two solutions in the chip inlets was 10 µL/h. After a few minutes, a stable gradient was generated and could be visualized and quantified through the imaging of fluorescent dextran.

Immunofixation in microchannels

Oxygen plasma treatment was performed only on the coverslip, so that the chip could be reversibly bound to glass. Cells were seeded in the chambers as detailed above and incubated for 12 hours at 37°C. The PDMS chamber was then immersed in a 3% PFA solution for 1 h at room temperature. The chip was carefully removed with a scalpel and tweezers. The cells were then permeabilized with 0.5X Triton for 3 min and subsequently incubated with staining agents. Phalloidin-AlexaFluor488 1:200 (Invitrogen, cat. A12379) was used to visualize actin, and DAPI 1:1000 (Sigma, cat. 32670) was used to visualize nuclei.

Time-lapse Microscopy

For migration assays testing the bias and the computation of $< p >$, a standard phase-contrast microscope was used, with a low-magnification objective (10x, N.A. 0.4) and a time interval of 10 min.
Nuclear deformation was imaged with an epifluorescence lamp (FluoArc Hg Lamp) coupled with a UV fluorescence filter. To do so, cells were incubated with DAPI (4 µg/mL).
Actin bundles during migration were visualized with lifeAct-mCherry under the same epifluorescence microscope with a 40x oil objective (N.A. 1.3).
We visualized and tracked focal contacts with a stable NIH3T3 cell line expressing VASP-GFP.
Finally, the keratin network in Cal-27 cells was visualized with a Nikon Spinning-Disk confocal microscope with a 60x oil objective (N.A. 1.4) using the Perfect Focus System.
Cell trajectories are generated by tracking the nucleus over time.

Cancer cell lines for keratin: K14 and V7 fusion variant

Gene segments of wild-type keratin 14 (K14) and fusion variant 7 (V7) were amplified from oral cancer cells via nested PCR and subcloned into the pAcGFP1-N1 vector (Clontech Lab., Madison. WI) as previously described [20]. Because the main backbone of V7 is K14, K14 was utilized as the wild-type control. The vector constructs were further transfected into the CAL27 oral squamous cell line purchased from the Bioresource Collection and Research Center (BCRC, Taiwan). The positive clones were enriched by cell sorting and maintained by G418 selection (700 µg/ml). Stable clones were generated by limiting dilution.

Statistics

Kolmogorov distribution comparisons were performed with Origin Pro.

Polarity measurement

As a read-out for anisotropy in keratin (Fig. 2e-f), we defined the norm of the polarity, $\vec{p}$, as follows:

$$|\vec{p}| = \int_0^{S_a} I_a - \int_0^{S_b} I_b$$

where I is the fluorescence intensity, and S is the surface. The cell is divided into two regions, a and b, by its center of mass.

Velocity fields

Velocity magnitude maps from Figure 3 have been extracted with PIVlab1.4.

RESULTS

Local asymmetry and entry point bias cell motion in two different confined situations

To mimic the blockage of cells such as CTCs in small veins, we designed microfabricated channels with periodic asymmetries to bias polarity and rectify cell motions through *ratchetaxis*. In designing the channels, we tested different conditions with various bottleneck sizes and angles. Under strong confinement, cells were not able to move; otherwise, the nuclei were less 'squeezed' (Figure S1). The best balance between optimal confinement and sustained migration was obtained for the 'a16i4' condition, where *a* corresponds to the tip angle (in degrees) and *i* to the opening width (in µm). In addition, the bottleneck width (4 µm) was always narrower than the nuclei, ensuring that cells would deform independent of their stage in the cell cycle (see Figure S1c).

Two sets of configurations were considered (Figure 1a) to evaluate the potential effects of full confinement: open channels, in which cells were only confined by the sides of the channels (Movies S1 and S2), and closed channels, in which cells were totally confined (Movies S3 and S4). Under each condition, ratchets were compared with linear channels whose dimensions were determined by the width, *i*, of the ratchet constriction (see Figure 1b bottom).

NIH3T3 cells were able to move along the channels throughout the experimental period (12 h) (Figure 1b and Movies S1-S4). As in *ratchetaxis* on topographical motifs, the nucleus seemed to be the large organelle preventing cell passage, as assessed by pauses in the phases of motion recorded in the ratchet, which were absent when cells moved along linear channels (Figure 1c). Deformation of the nucleus was clearly visible in our experiments (Figure 1c and Movie S5) in different cell types (Figure 2e and Figure S2).

In the open channel configuration, cells were rectified along the direction of the ratchet (Movie S1), consistent with ratchet configurations probed in previous studies [21–24,27,29]. This is shown by the mean displacement vector (Figure S3). The bias is also characterized by the measurement of the mean bias per step, *p*, defined as follows:

$$p = \frac{n_+ - n_-}{n_+ + n_-} \qquad (1)$$

where n_i corresponds to a step (in lattice unit) made in the *i* direction; i = + if the cell moves towards the tip of the ratchet, and i = - if the cell moves towards the base of the ratchet [27]. This parameter provides a clear readout of the bias in cell migration and indicates a

significant difference between cell motion in ratchets and straight channels in open configurations (Figure 1d).

Surprisingly, cells that are fully confined exhibit persistent migration depending only on the broken symmetry *of the entry point*, with no sensitivity to the ratchet orientation thereafter (Movies S3 and S4). It appears that at least within the channel length probed in our devices, cells maintain their motion throughout the channel in both directions, leading to distributions of *p* peaking at approximately 1 and -1, depending on the entry point position (Figure 1d). This result suggests that entry might be critical when transposed to *in vivo* situations: when cells enter a capillary that is sufficiently small, repolarization will be impossible, and the direction of motion will be maintained– and in the absence of a chemical gradient.

Actin, focal adhesions and keratin accumulate at bottlenecks

Next, we focused on closed configurations, viewing this set up as the closest to *in vivo* situations. We asked how cells could pass the bottlenecks of ratchets. We imaged the localization and dynamics of the actin cytoskeleton, intermediate filaments and focal contacts. Stress fibers were present below and above the nucleus, as in topographical ratchets (Movie S6, Figure 2a-b and [24]). Focal contacts were also observed (Movie S7 and Figure 2c-d). However, they specifically accumulated after the ratchet bottleneck (Figure 2c-d). The distributions of these markers are established hallmarks for local stress generation. We hypothesize that cells anchor and 'pull' locally to deform the nucleus, which allows cell passage. The sequences of such correlations between cellular structures and cell motion are reported in Figure 2 and in Movies S6-S7.

Defects in the keratin cytoskeleton have been reported to be involved in some squamous cancers [20], but no analyses of their dynamics or migratory assays have been reported thus far. To determine whether defects in keratin impair motion in confined spaces, we used CAL27 oral squamous epithelial cells expressing wild-type keratin tagged with GFP. We also used a CAL27 mutant expressing a keratin fusion protein involved in squamous cancers. For both cell lines, no net motion was recorded on flat coverslips, as expected for epithelial cells. However, the WT cells could enter closed ratchets and migrate efficiently, confirming the difference in migratory behaviors between flat and 3D environments. Strikingly, in these cells, keratin was a dynamic structure with strong anisotropies in its distribution (see Movie S8 and Figure 2e). The accumulation of keratin was visible at the posterior of the nucleus when the cell passed through the bottleneck (Figure 2e). This was quantified by the measurement of polarity as a readout of the anisotropy in the keratin distribution (see Figure 2e-g). However, in the mutant strains expressing the keratin fusion protein, the keratin network was isotropic (Figure 2f-g). Interestingly, these cells were arrested at the bottleneck and did not move to the next ratchet unit (Movie S9 and Figure S4a). We verified that the nuclei had similar dimensions in the wild-type cells and in the mutants (Figure S4b), which suggested that the defects in intermediate filaments were correlated with arrest. Interestingly, the fusion cell line showed no, or only very small, structured keratin arrays surrounding the nucleus, and the nucleus was frequently fragmented (Figure S4a). This suggests that the dynamics of the keratin cytoskeleton are also important for the deformation and the maintenance of the integrity of large organelles such as nuclei, which sheds light on the potential involvement of intermediate filaments in the dynamic remodeling of cellular organelles. The fact that this fusion protein has been identified in squamous cancer suggests that cells could be blocked within small capillaries, allowing them to probe the endothelial layers and potentially penetrate tissues [30,31].

Topographical anisotropy impacts cell motion after gradient removal

We next combined motion in closed channels with *chemotaxis* to observe the potential interplay between topological and chemical cues: competition and cooperation have been reported between different types of gradients, and combined cues can lead to compensation or greater bias in cell motion on average [32–34]. We designed assays in which cells faced a serum gradient of 0.1% to 10% (see Methods). The gradient and the slope of the gradient were quantified through the visualization of TRITC-dextran incorporated in the solution (Figure 3a). In both ratchet orientations, cells migrated towards the high serum concentration (Figure 3b). However, upon the removal of the chemical gradient, an unexpected effect appeared: cells oriented in the ratchet direction could move, while cells oriented in the opposite direction did not (Movies S10-11 and Figure 3c-e). We hypothesize that the polarity induced by a gradient could be distinct from the polarity induced by topography. Protrusive activity would be facilitated in the direction of the gradient. When suppressed, this sustained activity would proceed in the former gradient direction but would not be sufficient to untrap the nucleus – depending on the ratchet direction. This is illustrated by lamellipodial activity at cell edges, which is maintained while nucleus undergoes deformation (Figure 3e). Protrusion extension can also be associated with the deformation of the nucleus within the constriction. In the ratchet direction, nucleus passage would be facilitated.

We checked that the number of steps after gradients removal did not depend on the exposure time (Figure S5a) and we quantified the observed phenomenon: when we aligned all the trajectory sequences with respect to gradient removal, we observed that the ratio of velocities for each case, $\frac{\alpha_+}{\alpha_-}$, was approximately 10, confirming the difference in behavior with respect to the ratchet direction (Figure 3f). This was also illustrated by Figure S5b, showing the cell velocity as the number of steps per hour after gradient removal.

DISCUSSION

Our results show that the direction of cells in ratchet channels is characterized by two types of behavior. In open configurations, rectification occurs along the direction of the broken symmetry. In a closed configuration, the direction is set by the polarization induced by the entry of cells into channels. Focal contacts, actin, and keratin anisotropy are involved in motion, potentially allowing the passage of nuclei blocked at bottlenecks, in accord with other reports deciphering the molecular interplay between the cytoskeleton and the nuclear envelope [19,35]. Defects in keratin impair motion. Finally, chemical gradients can induce directed motion, and cells become sensitive to the asymmetry of confinement when the chemical gradient is removed. Taken together, these findings reveal a variety of simple rules for understanding cell motion in confined situations.

Confinement and high persistency

Amoeboid cells exhibit high persistence in straight channels [13,14]. Here, we report that the direction of mesenchymal cells is exclusively set by the channel entry point. This leads to highly persistent motion without repolarization. The fact that the trajectories of cells in our assays were not biased in totally confined channels could appear contradictory to previous works [29]. However, the experiments of Le Berre *et al* were designed to confine cells only in the z direction, with periodic squeezing zones. Therefore, the nucleus and the cell body could relax in all dimensions after each lattice unit. In our assays, cells were constantly squeezed in

the z direction and periodically in the x-y direction. This confinement might have been too strong to allow any repolarization, therefore screening out the effect of *ratchetaxis* in such configurations. This suggests that anisotropy in protein distributions can translate into anisotropy in the forces exerted on the substrate. As such, FAs and actin stress fibers are cytoskeleton components generating stresses. It has been shown that FAs exert a force per unit area of 5.5 $nN.\mu m^{-2}$ [36]. Bias in their distributions leads to bias in pulling forces. These anisotropies are important for nuclear compression through a bottleneck and eventual passage through the bottleneck.

Implication of ratchet-like channels *in vivo*

The extrapolation of these results to *in vivo* cases is an attractive possibility. The fact that capillaries of cell size have been reported [7,9] and that cell blockage is established in vessels suggests that confinement could be an important phenomenon in physiological situations. In this respect, the entry of cells into the channel and their subsequent motion could constitute a relevant assay for reproducing this situation *in vitro*. Single cells may probe their local environment, and the entry into a vessel could be related to the polarization rules reported in our study. This could involve topographical asymmetry, in which cells would probe the local environment, and/or exposure to changing chemical gradients, which may bias cells to move directionally. Future works could test this hypothesis in ratchet configurations and in cellular systems prone to respond to chemical gradients in cancer.

Keratin defects in cancer and blockage in capillaries

Our results from experiments involving the keratin fusion protein are interesting along these lines and regarding the implication of the protein in cancer. Cells could not pass bottlenecks under these conditions, which was associated with defects in the keratin network. Feedback exists between actin, polarity signaling and intermediate filaments, and it has been shown that intermediate filaments participate in the regulation of compressive forces during nuclear passage through narrow spaces [37,38]. As such, keratins and other intermediate filaments could be key players in cell motility in confined spaces. The fusion of keratin has been reported in medical cases, and further experiments conducted *in vivo* may confirm whether such impairment of cellular motion in capillaries is responsible for cancer spreading. Since initial arrest in the capillary is critical for tumor cells to metastasize to secondary sites in distant organs, the blockage of migration by keratin fusion may provide advantages for tumor seeding, survival and proliferation [30,31]. The type of impaired migration addressed here would be distinct from the entry of cells from primary tumors into blood vessels, in which protease-mediated matrix remodeling plays a greater role.

Competition between topography and chemotaxis

The results of the gradient experiment were puzzling. There seems to be increased sensitivity related to exposure to chemical gradients. Polarity cues in the cortex may lead to a local increase in surface tension. As a result, subsequent motion in the presence of an obstacle could be affected depending on the direction of topographical anisotropy. This is consistent with previous works showing that cells migrate along the path of least resistance [39]: an increase in cortical tension due to gradient exposure might be deleterious to cell passage when the topographical anisotropy opposes cellular motion. These gradient experiments suggest that distinct pathways may be triggered by chemical and mechanical gradients.

Micro-channels experiments versus Boyden chambers

Finally, this study suggests that channels may be more relevant to the study of invasion than standard tests, for example, with Boyden chambers [40]. In the latter case, chemical gradients are located between two reservoirs, and the passage of cells, such as fibroblasts or epithelial cells, is tested through thin cavities whose dimensions are a fraction of the size of a cell. Such a configuration would seem to be far from *in vivo* conditions. Future studies could use these ratchet channels to identify molecular actors and signaling networks related to cancer cells, along the lines of the strategy reported in this study for squamous cancer cell lines.

REFERENCES

1. Carmona-Fontaine, C., Matthews, H. & Mayor, R. Directional cell migration in vivo Wnt at the crest. *Cell Adh. Migr.* **2**, 240–242 (2008).
2. Machesky, L. M. Lamellipodia and filopodia in metastasis and invasion. *FEBS Lett.* **582**, 2102–2111 (2008).
3. Wijnholds, J. 'Basal Cell Migration' in Regeneration of the Corneal Wound-Bed. *Stem Cell Reports* **12**, 3–5 (2019).
4. Stuelten, C. H., Parent, C. A. & Montell, D. J. Cell motility in cancer invasion and metastasis: insights from simple model organisms. *Nat. Publ. Gr.* **18**, 296–312 (2018).
5. Codling, E. A., Plank, M. J. & Benhamou, S. Random walk models in biology. *J. R. Soc. Interface* **5**, 813–834 (2008).
6. Bissell, M. J. Goodbye flat biology - time for the 3rd and the 4th dimensions. *J. Cell Sci.* **130**, 3–5 (2017).
7. Yamauchi, K. *et al.* Real-time in vivo dual-color imaging of intracapillary cancer cell and nucleus deformation and migration. *Cancer Res.* **65**, 4246–4252 (2005).
8. Rejniak, K. A. Circulating Tumor Cells: When a Solid Tumor Meets a Fluid. *Adv Exp Med Biol.* **936**, 93–106 (2016).
9. Caggiati, A., Phillips, M., Lametschwandtner, A. & Allegra, C. Valves in Small Veins and Venules. *Eur. J. Vasc. Endovasc. Surg.* **32**, 447–452 (2006).
10. Hawkins, R. J. *et al.* Pushing off the walls: A mechanism of cell motility in confinement. *Phys. Rev. Lett.* **102**, 1–4 (2009).
11. Liu, Y. J. *et al.* Confinement and low adhesion induce fast amoeboid migration of slow mesenchymal cells. *Cell* **160**, 659–672 (2015).
12. Maiuri, P. *et al.* Actin Flows Mediate a Universal Coupling between Cell Speed and Cell Persistence. *Cell* **161**, 374–386 (2015).
13. Faure-andré, G. *et al.* Regulation of Dendritic Cell Migration by CD74, the MHC Class II-Associated Invariant Chain. *Science.* **322**, 1705–1710 (2008).
14. Chabaud, M. *et al.* Cell migration and antigen capture are antagonistic processes coupled by myosin II in dendritic cells. *Nat. Commun.* **6**, 1–16 (2015).
15. Bodor, D. L., Pönisch, W., Endres, R. G. & Paluch, E. K. Of Cell Shapes and Motion: The Physical Basis of Animal Cell Migration. *Dev. Cell* **52**, 550–562 (2020).
16. Reversat, A. *et al.* Cellular locomotion using environmental topography. *Nature* **582**, 582–585 (2020).
17. Le Berre, M., Aubertin, J. & Piel, M. Fine control of nuclear confinement identifies a threshold deformation leading to lamina rupture and induction of specific genes. *Integr. Biol.* **4**, 1406–1414 (2012).
18. Halfmann, C. T. *et al.* Repair of nuclear ruptures requires barrier-to-autointegration factor. *J. Cell Biol.* **218**, 2136–2149 (2019).
19. Thiam, H. R. *et al.* Perinuclear Arp2/3-driven actin polymerization enables nuclear

deformation to facilitate cell migration through complex environments. *Nat. Commun.* **7**, 10997–11011 (2016).
20. Tsai, F. J. *et al.* Novel K6-K14 keratin fusion enhances cancer stemness and aggressiveness in oral squamous cell carcinoma. *Oncogene* **38**, 5113–5126 (2019).
21. Caballero, D., Voituriez, R. & Riveline, D. Protrusion fluctuations direct cell motion. *Biophys. J.* **107**, 34–42 (2014).
22. Caballero, D., Comelles, J., Piel, M., Voituriez, R. & Riveline, D. Ratchetaxis: Long-Range Directed Cell Migration by Local Cues. *Trends Cell Biol.* **25**, 815–827 (2015).
23. Caballero, D., Voituriez, R. & Riveline, D. The cell ratchet: Interplay between efficient protrusions and adhesion determines cell motion. *Cell Adhes. Migr.* **9**, 327–334 (2015).
24. Comelles, J. *et al.* Cells as active particles in asymmetric potentials: Motility under external gradients. *Biophys. J.* **107**, 1513–1522 (2014).
25. Mahmud, G. *et al.* Directing cell motions on micropatterned ratchets. *Nat. Phys.* **5**, 606–612 (2009).
26. Sun, X. *et al.* Asymmetric nanotopography biases cytoskeletal dynamics and promotes unidirectional cell guidance. *Proc. Natl. Acad. Sci. U. S. A.* **112**, 12557–12562 (2015).
27. Lo Vecchio, S. *et al.* Collective Dynamics of Focal Adhesions Regulate Direction of Cell Motion. *Cell Syst.* **10**, 1–8 (2020).
28. Le Maout, E., Lo Vecchio, S., Bhat, A. & Riveline, D. Directing cell migration on flat substrates and in confinement with microfabrication and microfluidics. *Methods Cell Biol.* **147**, 109–132 (2018).
29. Le Berre, M. *et al.* Geometric Friction Directs Cell Migration. *Phys. Rev. Lett.* **111**, 1–5 (2013).
30. Chambers, A. F., Groom, A. C. & MacDonald, I. C. Dissemination and growth of cancer cells in metastatic sites. *Nat. Rev. Cancer* **2**, 563–572 (2002).
31. Labelle, M. & Hynes, R. O. The initial hours of metastasis: The importance of cooperative host-tumor cell interactions during hematogenous dissemination. *Cancer Discov.* **2**, 1091–1099 (2012).
32. Prentice-Mott, H. V. *et al.* Biased migration of confined neutrophil-like cells in asymmetric hydraulic environments. *Proc. Natl. Acad. Sci. U. S. A.* **110**, 21006–21011 (2013).
33. Moreau, H. D. *et al.* Macropinocytosis Overcomes Directional Bias in Dendritic Cells Due to Hydraulic Resistance and Facilitates Space Exploration. *Dev. Cell* **49**, 171–188 (2019).
34. Belotti, Y., Mcgloin, D., Weijer, J. & Weijer, C. J. Chemotaxis overrides Barotaxis during Directional Decision-Making in Dictyostelium discoideum. *bioRxiv* 1–23 (2020) doi:10.1101/2020.01.14.904748.
35. Davidson, P. M. *et al.* Nesprin-2 accumulates at the front of the nucleus during confined cell migration. *EMBO Rep.* **21**, 49910 (2020).
36. Balaban, N. Q. *et al.* Force and focal adhesion assembly: a close relationship studied using elastic micropatterned substrates. *Nat. Cell Biol.* **3**, 466–472 (2001).
37. Bodegraven, E. J. Van & Etienne-Manneville, S. Intermediate filaments against actomyosin : the david and goliath of cell migration. *Curr. Opin. Cell Biol.* **66**, 79–88 (2020).
38. Leduc, C. & Etienne-Manneville, S. Regulation of microtubule-associated motors drives intermediate filament network polarization. *J. Cell Biol.* **216**, 1689–1703 (2017).
39. Renkawitz, J. *et al.* Nuclear positioning facilitates amoeboid migration along the path of least resistance. *Nature* **568**, 546–550 (2019).
40. Boyden. The Chemotactic Effect of Mixtures of Antibody and Antigen on Polymorphonucleaer Leucocytes. *J. Exp. Med.* 453–466 (1962)

ACKNOWLEDGMENT

We thank J. Comelles, E. Pencreach, O. Pertz, P. Rossolillo, the Imaging Platform of IGBMC, the Riveline Lab. for help, constructs and discussions. We acknowledge Raphaël Voituriez for his comments on the manuscript. This study with the reference ANR-10-LABX-0030-INRT has been also supported by a French state fund through the Agence Nationale de la Recherche under the frame programme Investissements d'Avenir labelled ANR-10-IDEX-0002-02. D.R. acknowledges funding from Région Grand Est, Alsace contre le cancer, the University of Strasbourg and the CNRS.

Figure Captions

Figure 1. Cell motility in 3D ratchets. (a) Configurations tested in this study. Two types of confinements are produced: side-only confinement, with open channels, and full confinement, with closed channels. Ratchets are defined as "+" when cells are directed towards the tip of the ratchet and "-" when cells are directed against the tip of the ratchet. (b) Cells migrate in ratchets and in straight channels. Here, open channels are shown. Scale bars: 20 µm. (c) The nucleus has to deform to pass the bottleneck in closed configurations, leading to decreases in velocity corresponding to pauses (red arrows). In straight channels, the velocity is almost always nonzero, and migration is facilitated. Scale bar: 10 µm. (d) The mean bias per step, *p*, as a function of the tested conditions. In open configurations, cells migrate preferentially in the "+" direction. In closed channels, cells are totally biased by the entry point, with no change in direction, resulting in distributions peaking at 1 and -1. Significance was tested through the comparison of distributions using a Kolmogorov test; p = 0.02*.

Figure 2. Anisotropies in the cytoskeleton correlate with nuclear deformation. (a) NIH3T3 cells in a closed ratchet. Staining shows actin and nucleus. Arrows indicate actin bundles at the top and at the bottom, surrounding the nucleus deformed at the bottleneck. (b) Lifeact-mCherry live imaging. Actin bundles are present throughout the motion of the cell. (c) VASP-GFP in NIH3T3 cells. Focal contacts are mainly present at the bottom of the bottleneck and in the protrusions extended by cells. (d) Visualization of protrusion growth with VASP-GFP. Focal contacts mainly undergo nucleation at the interface between the wall and the surface. (e) K14-GFP showing the keratin cytoskeleton in CAL27 oral squamous cells with its anisotropy map. Keratin is distributed at the posterior of the nucleus during its passage through the bottleneck. (f) The CAL27-expressing modified keratin fusion protein with its anisotropy map. (g) Quantification of the norm of polarization, $\vec{p}$, for WT K14-GFP (top) and for the keratin fusion protein (bottom). Scale bar = 15 µm in all panels. Time in hh:mm.

Figure 3. Combination of *ratchetaxis* and *chemotaxis*. (a) Phase-contrast image of a straight channel (closed) with a serum gradient. The gradient is visualized with TRITC-dextran, and the slope can be extracted. (b) NIH3T3 moving towards a high serum concentration. The contour of the nucleus is shown in blue. (c) After gradient removal, the cell ceases motion when it moves against the ratchet direction. When the cell faces the ratchet orientation (d), it continues to move after gradient removal. For (b), (c) and (d), t_0 corresponds to cell entry in the channel. (e) Nuclear motion of the cell presented in (c). After gradient removal, the nucleus is blocked at the bottleneck, preventing cell passage. Lamellipodia and nuclei are outlined in white and blue, respectively. Motion of lamellipodium at the front can be associated with nucleus deformation (left). The x-component of the velocity field is shown in the associated heat map (right). Red indicates motion in the ratchet direction ("+"); blue indicates motion against the ratchet direction ("-"). Note that activity at cell edges continues after gradient removal while the nucleus moves back and forth against the bottleneck. (f) Cells positions

along the x-axis aligned with the removal of the gradient (dashed blue line). Slopes are extracted from the linear fits after gradient removal, and the respective coefficients are displayed in the plot. Cells in the orientation of the ratchet (+) can migrate, whereas the migration of cells in the opposite direction stops (-).

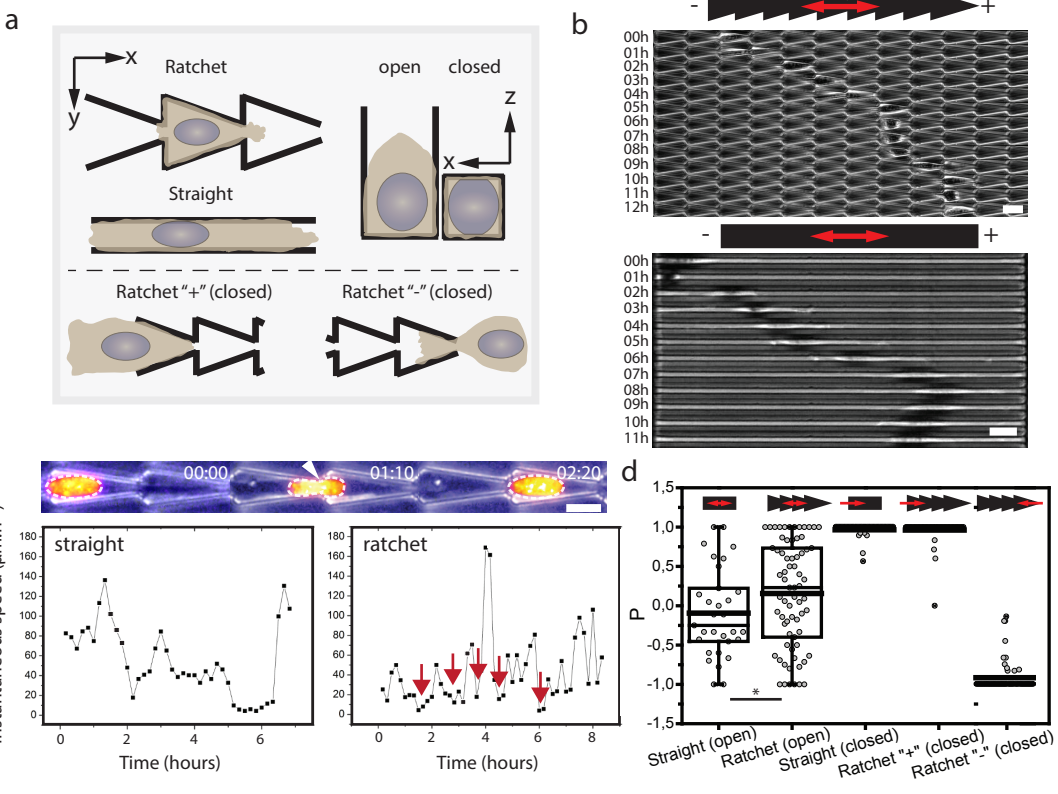
a
x
y
Ratchet
open
closed
z
x
Straight
Ratchet "+" (closed)
Ratchet "-" (closed)
b
-
+
00h
01h
02h
03h
04h
05h
06h
07h
08h
09h
10h
11h
12h
-
+
00h
01h
02h
03h
04h
05h
06h
07h
08h
09h
10h
11h
c
00:00
01:10
02:20
straight
ratchet
Instantaneous speed (µm.h-1)
Time (hours)
Time (hours)
d
P
Straight (open)
Ratchet (open)
Straight (closed)
Ratchet "+" (closed)
Ratchet "-" (closed)
*

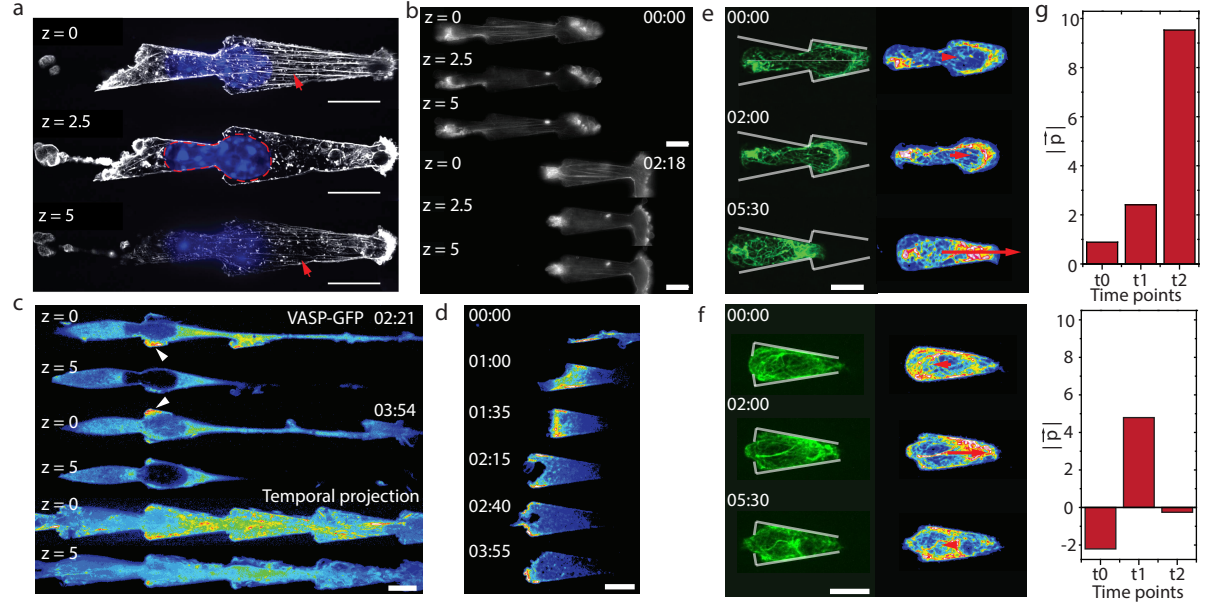
a
z = 0
z = 2.5
z = 5
b
z = 0
00:00
z = 2.5
z = 5
z = 0
02:18
z = 2.5
z = 5
e
00:00
02:00
05:30
g
10
8
6
4
2
0
$|\vec{p}|$
t0
t1
t2
Time points
c
z = 0
VASP-GFP 02:21
z = 5
z = 0
03:54
z = 5
z = 0
Temporal projection
z = 5
d
00:00
01:00
01:35
02:15
02:40
03:55
f
00:00
02:00
05:30
10
8
6
4
2
0
-2
$|\vec{p}|$
t0
t1
t2
Time points

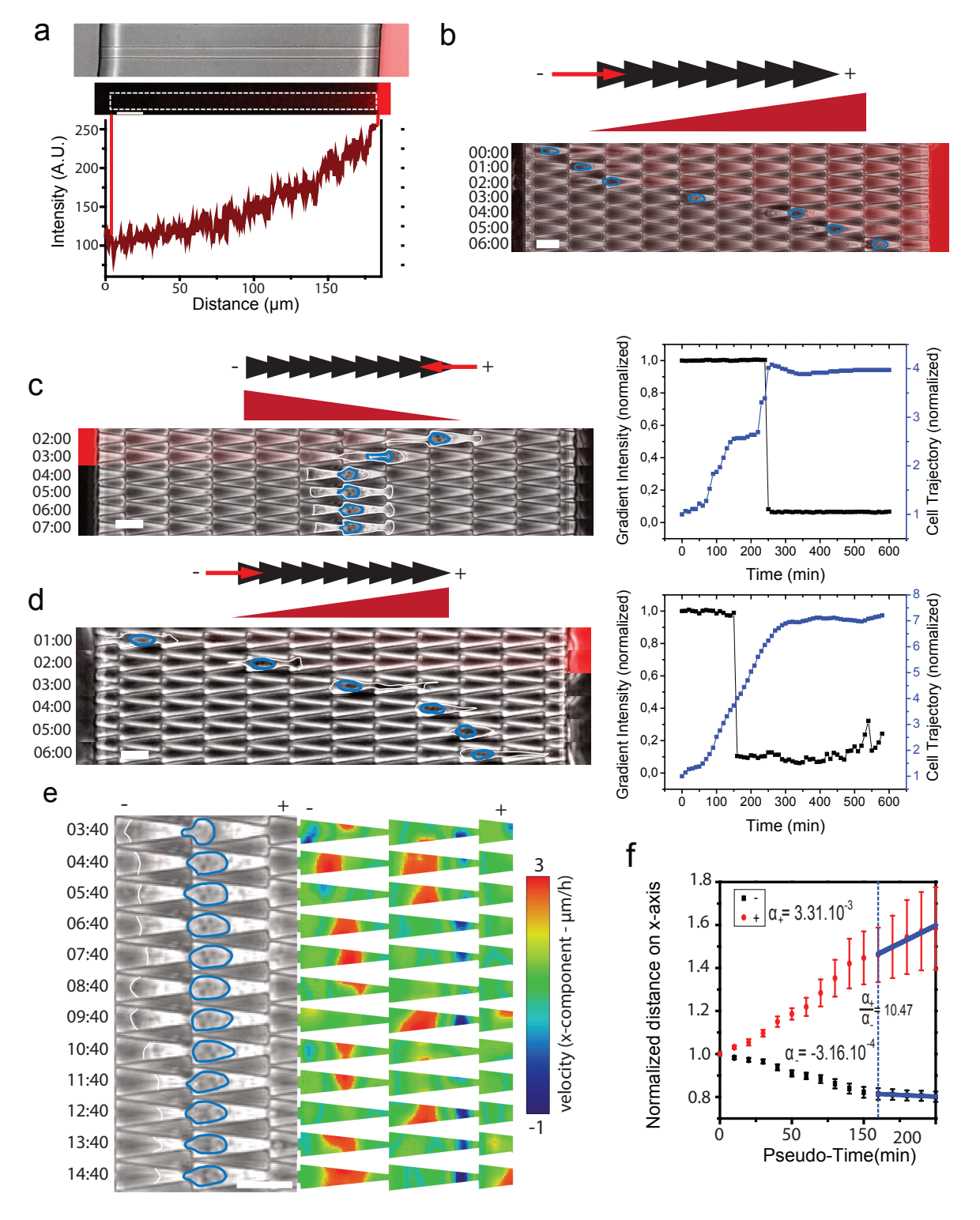
a
Intensity (A.U.)
250
200
150
100
0
50
100
150
Distance (µm)
b
-
+
00:00
01:00
02:00
03:00
04:00
05:00
06:00
c
-
+
02:00
03:00
04:00
05:00
06:00
07:00
Gradient Intensity (normalized)
Cell Trajectory (normalized)
Time (min)
d
-
+
01:00
02:00
03:00
04:00
05:00
06:00
Gradient Intensity (normalized)
Cell Trajectory (normalized)
Time (min)
e
-
+
-
+
03:40
04:40
05:40
06:40
07:40
08:40
09:40
10:40
11:40
12:40
13:40
14:40
3
-1
velocity (x-component - µm/h)
f
Normalized distance on x-axis
α+= 3.31.10-3
α-= -3.16.10-4
α+ / α- = 10.47
Pseudo-Time(min)